Relatório Final de Pesquisa - CNPq

Fabrication of hybrid SiC and nanodiamond particles with immobilised photoreceptors and their bio-analytical application for controlled drug delivery

Part 1. Preparation of silicon carbide with high surface area

Pesquisador: Dr. Mykhailo Nazarkovskyi

Processo CNPq: 154011/2016-9

Rio de Janeiro, novembro de 2017

1. Abstract

Commercial powder and SHS-synthesized silicon carbide nanowires were studied. Nanodots of gold were deposited onto a surface of a powder SiC. Basic properties, such as crystalline structure, phase composition, morphology and photocatalytic activity of all three materials types have been determined. Obtained silicon carbides are crystalline materials of hexagonal (commercial raw and gold modified SiC) and cubic (SiC nanowires) structures. No gold phase has been detected as a separate crystalline phase. The average size of finely distributed Au nanodots is at 3.5 nm at the concentration of 0.64 wt.%. The nanowires have been indicated to be active in a hydrogen generation and the CO_2 reduction to CO and CH_4. The gold-containing SiC demonstrated an essential enhancement of photocatalytic activity in a gas phase, as opposed to non-modified SiC powder. An extremal profile of the kinetics curve for the nano-sized gold-silicon carbide system is an evidence of parallel reactions occurrence with a selective shift of the equilibrium on the reaction media interface.

2. Introduction

Silicon carbide is an outstanding ceramic which has diverse industrial applications due to high hardness and strength, thermal stability, high melting point, oxidation resistance, high erosion resistance. It is a component of catalytic systems, epoxy-composites, electrical and semiconductor devices.

Approximately 250 crystalline structures of SiC have been discovered and studied. Some research groups indicated that SiC polytypes featured in the seed orientation in terms of crystallography, whereas this phenomenon was supposed to be associated with different surface energies of Si and C faces. The most common polytypes are listed as 3C (cubic F43m, E_g = 2.3 eV), 4H (hexagonal P63mc, E_g = 3.2 eV) and 6H (hexagonal P63mc, E_g = 3.0 eV) form (Fig. 1).

A large variety of papers was published on SiC synthesis since its production was initiated in 1892 – depending on a form, different ways to manufacture SiC are considered. The most commonly used methods for SiC synthesis are physical vapour deposition (PVT), chemical vapour deposition (CVD), sol-gel, liquid phase sintering (LPS) or mechanical alloying (MA).

The present stage comprises studies on physicochemical properties of commercial SiC powder, gold-modified commercial SiC and SiC nanowires synthesized by Huczko *et al.* via Self-Propagating High-Temperature Synthesis (SHS) [1–3]. In this preliminary study, nano-sized gold was chosen as a typical electron sink to be implicated for multi-electron processes.

Another aspect of *nano*-SiC analysis addressed with the present research consists in the ecological issues solution caused by a "green house" effect due to CO_2 accumulation in the atmosphere. The ability of SiC to act as a photocatalyst is attributed to predicting interface interactions mechanisms. To understand the processes of chemisorption associated with WP3 and WP4, we are undertaking "pilot" testing of SiC interface activity.

The CO_2 reduction subject was thoroughly studied and all possible mechanisms of a stepwise reduction of carbon dioxideare determined predicting standard redox potentials [4–6]:

Reaction	**E^0, V (pH = 7)**
$CO_2 + 2e- \rightarrow {}^{\bullet}CO_2^-$	−1.90
$CO_2 + 2H^+ + 2e^- \rightarrow HCOOH$	−0.61
$CO_2 + 2H^+ + 2e^- \rightarrow CO$	+−0.53
$CO_2 + 4H^+ + 4e^- \rightarrow HCHO$	+−0.48
$CO_2 + 6H^+ + 6e^- \rightarrow CH_3OH$	+−0.38
$CO_2 + 8H^+ + 8e^- \rightarrow CH_4$	+−0.24
$2H_2O + 4h^+ \rightarrow O_2 + 4H^+$	+0.81
$2H^+ + 2e^- \rightarrow H_2$	−0.42

As seen, within the full reduction scheme of $CO_2 \rightarrow CH_4$, multifold organic intermediates at different ratios may be formed and collected in a liquid phase. Thus, it is of key importance to analyze not only gas products (CO, CH_4 or H_2), but also organic derivatives (methanol CH_3OH, formaldehyde HCOH, formic acid HCO_2H).

In connection therewith, as a model reaction for catalysis, carbon dioxide reduction catalyzed by silicon carbides was run.

3. Materials and Methods.

As materials to be tested, commercial SiC powder (Sigma Aldrich, ≥97.5%,
400 mesh) (SiC SA) and raw SiC nanowires (SiC NW) were subjected for characterization and catalytic studies.

Commercial SiC was heated in a HNO_3 : HF (3:1 v/v) mixture inside a PTFE jar during 1 h. After heating, the suspension was maintained for 24 h, diluted with DW, filtered, washed with DW to neutralize acids residues and dried at 50 °C. Obtained sample was labeled as SiC SA.

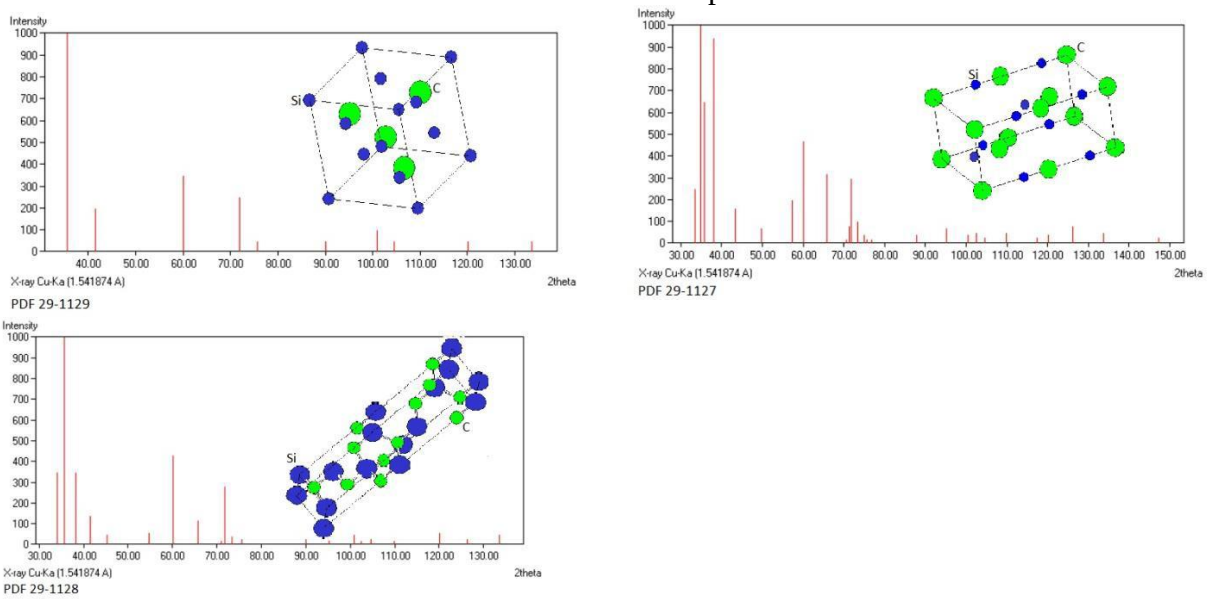

Fig. 1. XRD patterns of 3C (a), 4H (b) and 6H (c) crystalline polytypes of Si C with respective lattice configuration.

A designed technique of Self-Propagating High-Temperature Synthesis (SHS) was used to obtain SiC NW. The concept of SHS lies in the exothermic, self-sustainable process initiated by the resistive heating of homogenous stoichiometric mixture of powdered silicon Si and polytetrafluoroethylene $-(CF_2)_n-$ at and terminated within few seconds (Fig. 2).

Fig. 2. The experimental set-up for SHS (left), the light signal emitted during combustion as an observation via polycarbonate window (middle), and raw sponge-like product (right).

In addition, the sodium azide NaN_3 was introduced (55 wt.%) to enable forming of bundles.

The reaction was carried out under the air atmosphere and assumed to occur through two ways:

$2\ Si + 2\ –(CF_2)– = SiF_4\uparrow + C + SiC$

$2\ NaN_3 + 3\ Si + 3\ –(CF_2)– = 2NaF + C + 2SiC + 3N_2\uparrow + SiF_4\uparrow$

The purification of SiC NW was carried out as follows: raw black nanowires were placed into KOH solution (30 wt.%) and heated at 70-80 °C inside a PTFE jar during 2 h, whereupon cooled down to the room temperature. Obtained alkali suspension was diluted by triple portion (v/v) of distilled water (DW), filtered and washed wth DW under vacuum on a Buechner funnel until pH = 7. Neutralized nanowires were calcined at 680 °C during 2 h. Obtained material had a grey color.

The metal colloids were prepared by sputter deposition on the SiC SA to fabricate Au@SiC SA. The deposition was performed in a sputter coater MED 020 (Bal-Tech), pre-evacuated at 10^{-3} Pa with discharge currents 40 mA for (time), under an argon work pressure of 2 Pa at room temperature. The mass of was measured (1 g) in a cylindrical glass support (3 cm diameter) and placed in the sputter coater horizontally. The SiC NW's surface was located at a distance of 50 mm from the gold target (99.99% in purity). The control of deposition rate was performed in situ by a quartz crystal film thickness measurement device (QSG 060- Bal-Tech).

The X-Ray diffraction (XRD) patterns were recorded through the use of a D8 Discover DaVinci diffractometer (Bruker, CuK_α, $\lambda = 0.154$ nm).

SEM images were recorded using a JSM-6700F scanning electron microscope (JEOL), TEM images of Au@SiC samples were made by dint of a JOEL JEM.

The content of gold nanodots on a surface of SiC powder was determined via ICP MS (NexION® 2000, Perkin Elmer).

To analyze textural properties of SiC NW, SiC SA, and Au@SiC SA (S_{BET}, porosity), low-temperature N_2 adsorption–desorption (Micrometrics ASAP 2020) was used. The total pore volume, V_p, was determined at the maximal adsorption point, i.e. at $p/p_0 = 0.98$- 0.99. Specific surface area, S_{BET}, was calculated from the standard BET method described in and parameters of textural porosity, e.g. incremental pore size distribution (IPSD), were estimated by application of the self-consisted regularization (SCR) under non-negative conditions of the pore size distribution function, i.e. $f(R_p) > 0$ at any pore radius R_p and at the set regularization parameter a = 0,01. It should be pointed out that the pores are viewed as voids among nanowires aggregates formed after calcination. The method allows us to estimate the contributions of different pore types based on their size hierarchy: nanopores (V_{nano} at $R_p < 1$ nm), mesopores (V_{meso} at 1 nm < R_p < 25 nm)

and macropores (V_{macro}, $R_p > 25$ nm) by usage of the distribution function $f_V(R_p)$ [7–11].

The photocatalytic CO_2 reduction was performed under a 300 W Xe-lamp irradiation in the presence of 20-30 mg of a catalyst (SiC, Au@SiC or SiC NW) suspended in 2 mL of liquid H_2O saturated with CO_2 during 30 min. The gas phase was sampled manually five times and analyzed on an gas chromatograph (Agilent, 6890N) detecting CO, H_2 or CH_4 generation.

4. Results and Discussions

The XRD patterns demonstrate formation of different crystalline phases. If SiC NW features in pure cubic SiC 3C, the commercial sample of SiC powder contains two hexagonal phases, 4H and 6H with domination of the 6H configuration (Fig. 3). All the samples do not contain amorphous phase and Au reflexes are not represented on the diffraction diagram (Fig. 4).

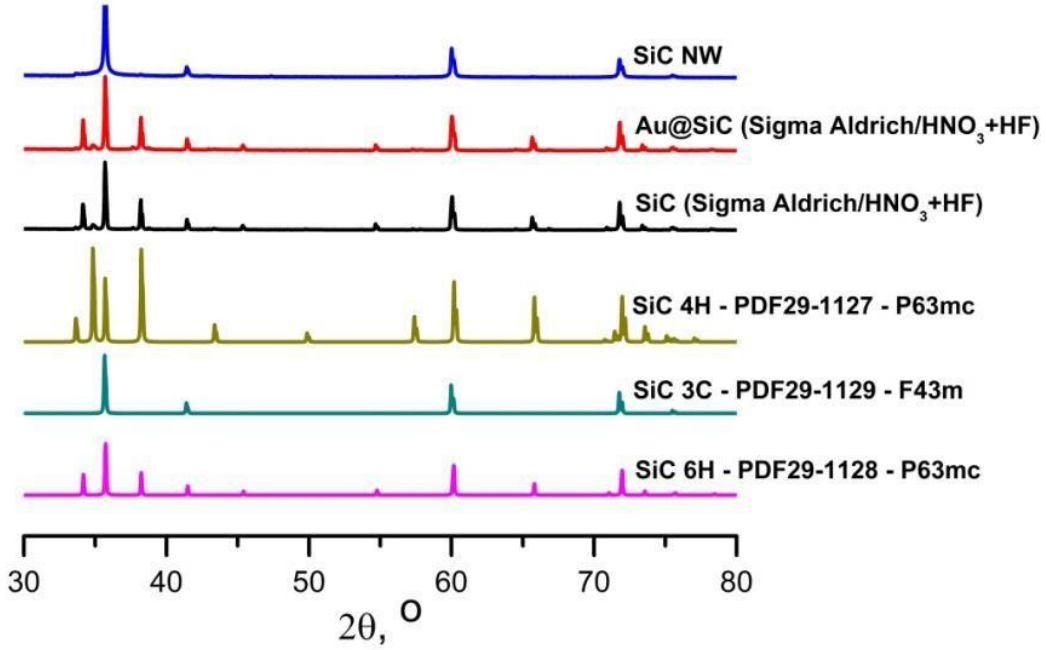

Fig. 3. XRD patterns of SiC NW, Au@SiC SA, SiC SA and crystalline standard phases: SiC 4H, SiC 3C and SiC 6H.

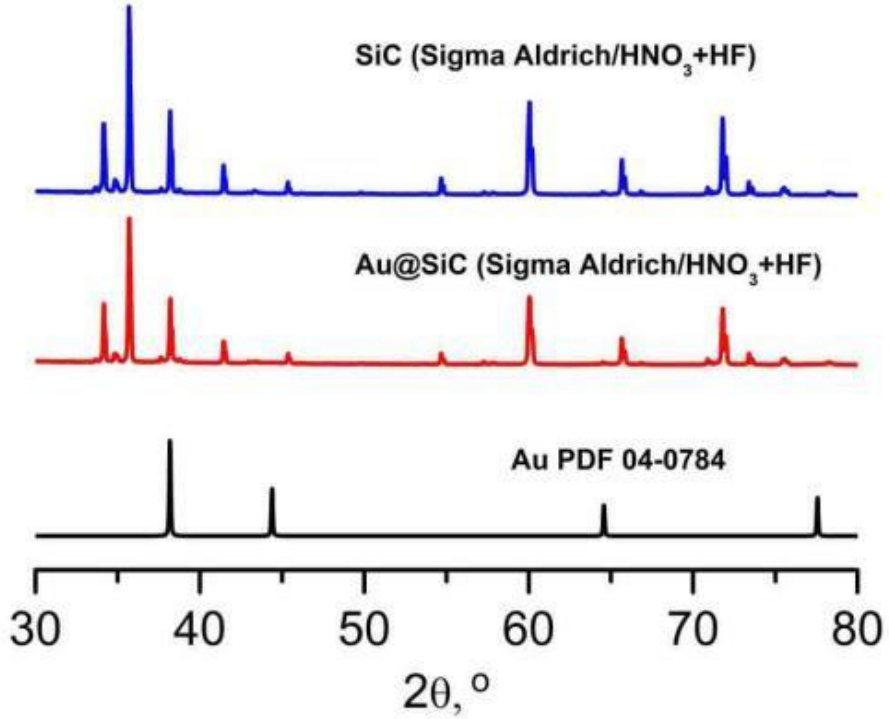

Fig. 4. XRD patterns of SiC SA, Au@SiC SA and crystalline standard Au.

The model of cylindrical, slit-shaped pores and voids between nanowires was based on the results of SEM studies. The latter show us significant gaps among anisotropic bodies of nanowires (Fig. 5). Due to the anisotropy, the interparticle porosity is not expected to be responsible for textural properties of SiC NW. They exhibit majority of mesopores (58.9%), but the macropores' share is at 37.7 %. This is because of the consolidation of raw amorphous carbon-contaminated nanowires calcined at 650 °C. This supports the view on the semilogarithmic pore size distribution scaled on Fig. 6.

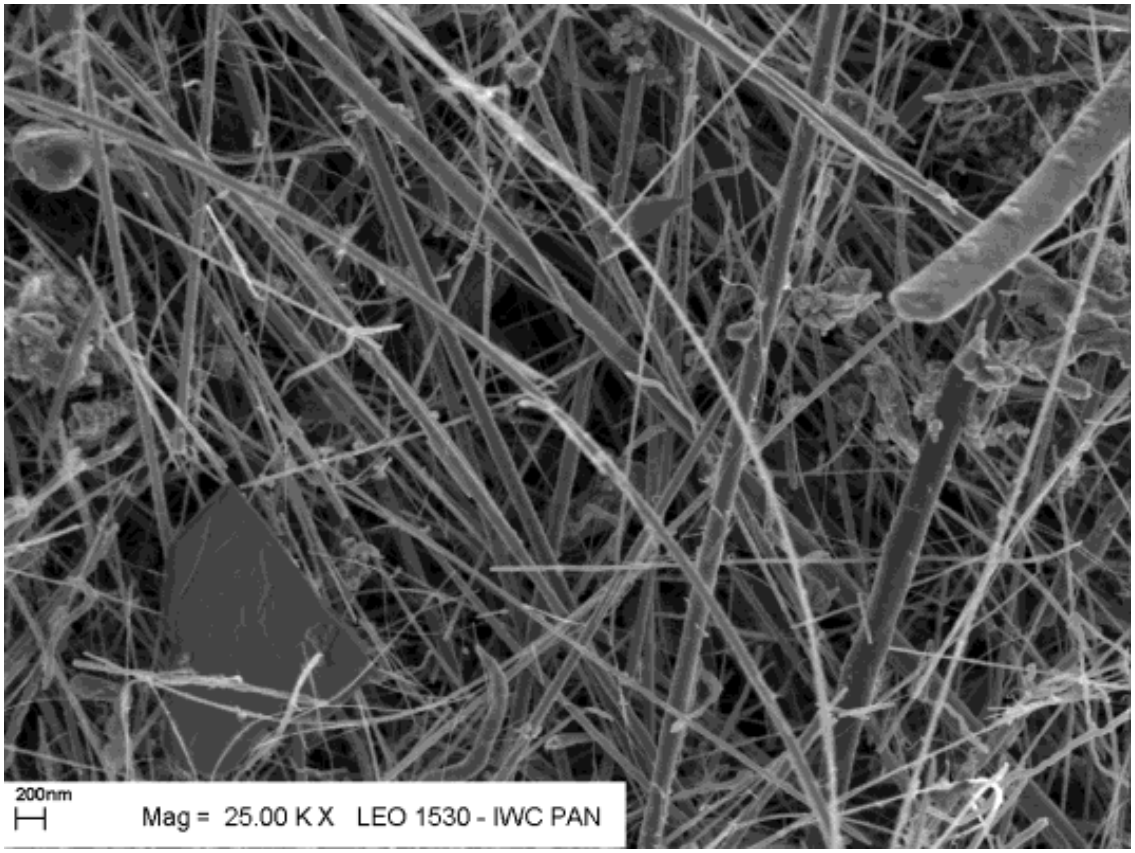

Fig. 5. SEM image of SiC nanowires calcined at 650 °C (2 h)

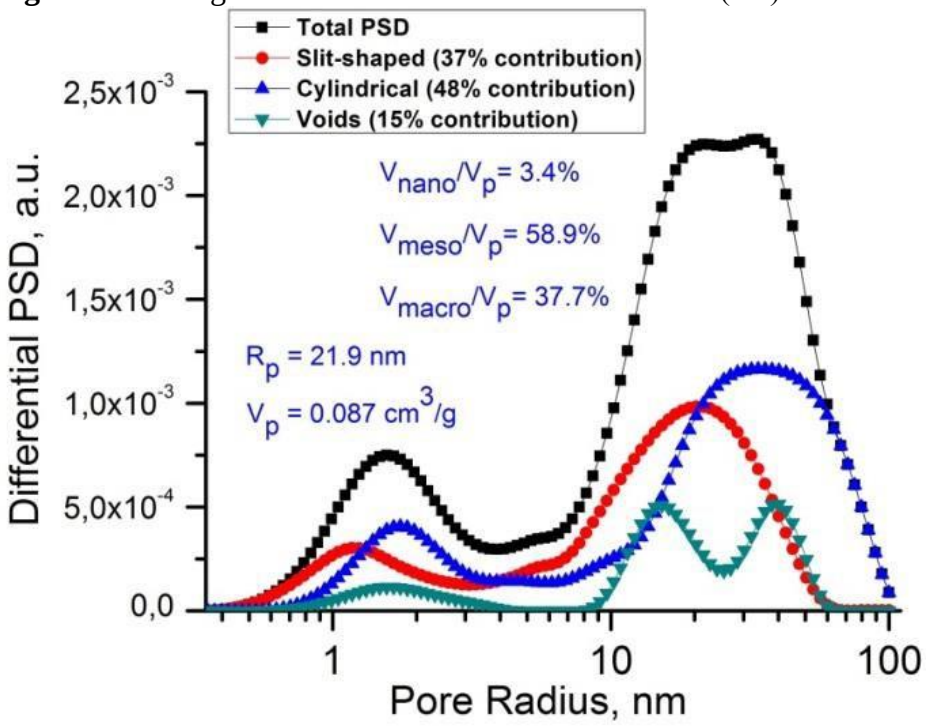

Fig. 6. The pores size distribution of SiC NW with contributions of different pores by shape.

As was suggested above, the contribution of voids is small, whereas cylindrical and slit-like pores are the most important – their occurrence is due to assembled packing of nanowires.
The processed SiC powder does not exhibit any change either in the surface morphology (Fig. 7) or porosity - S_{BET} = 1 m^2/g.

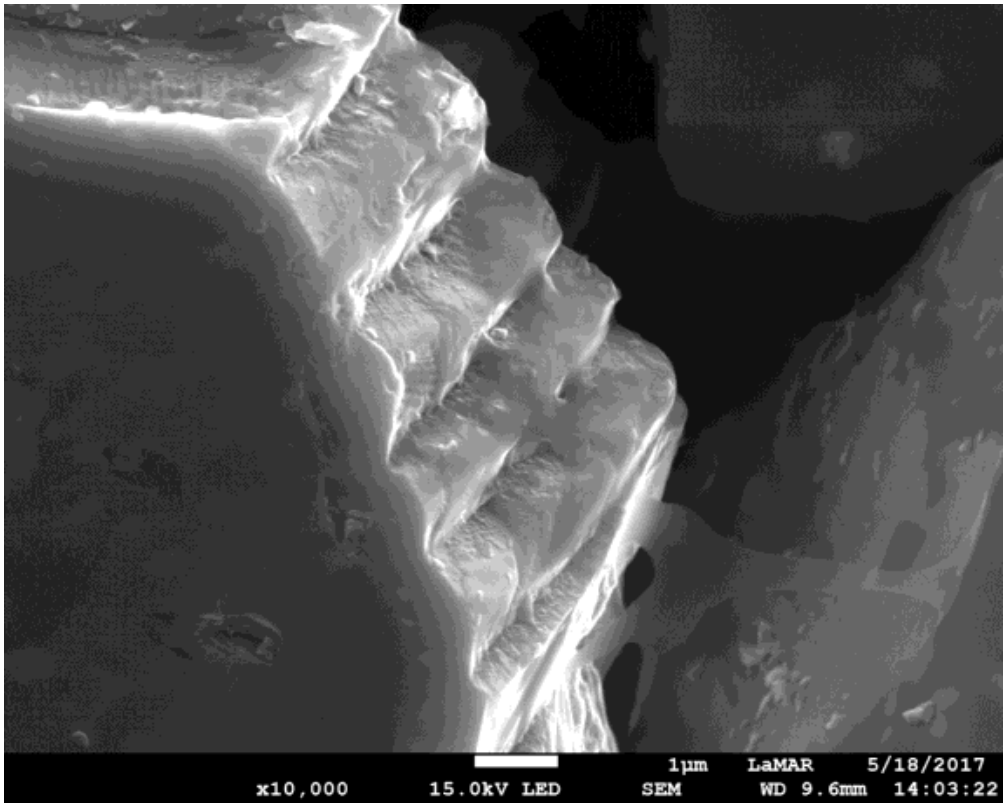

Fig. 7. The SEM image of commercial SiC powder processed by HNO_3 + HF

The concentration of Au in Au@SiC SA is 0.64 wt.%, whereas the average particle size is 3.5 nm (Fig. 8). At room temperature Au nanoparticle do not tend to aggregation. And during heating or mechanical impact, they can migrate leaving a surface or aggregating.

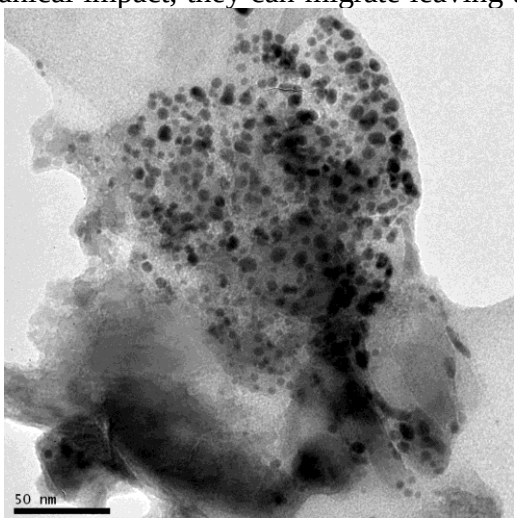

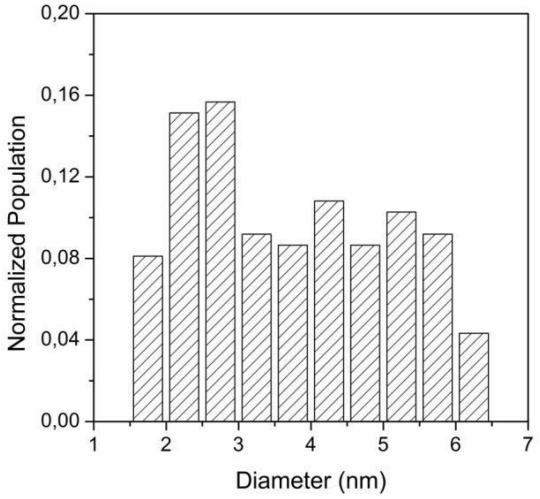

Fig. 8. The TEM image of Au@SiC SA *(a)*, and normalized gold particles size distribution *(b)*

The kinetics studies results of CO_2 reduction are shown below. In a gas phase collected over a liquid reaction medium, we have detected methane CO, CH_4 and H_2 as products of the reduction process (Fig. 9).

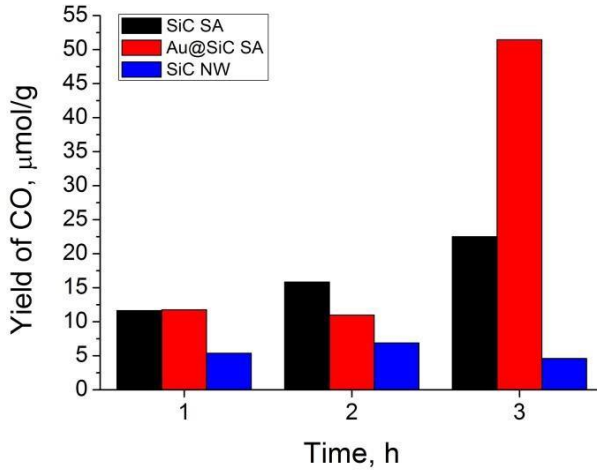

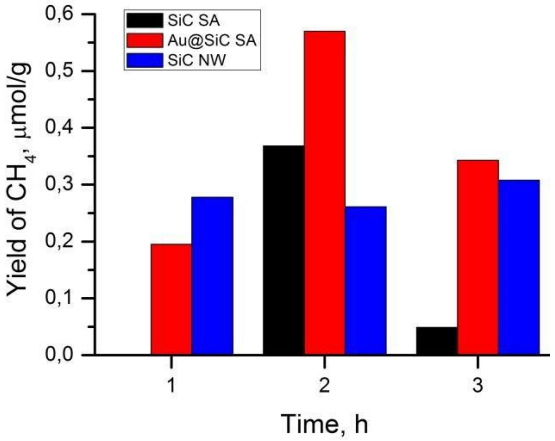

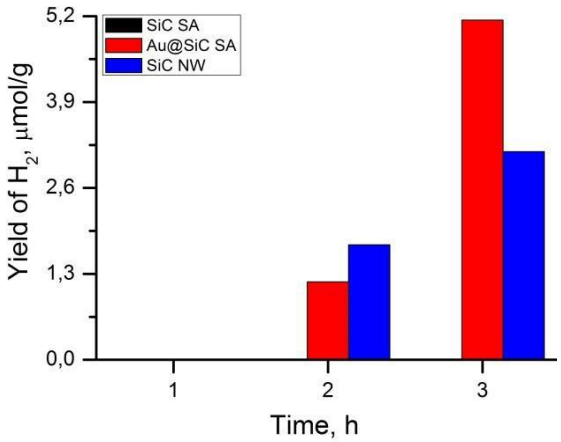

Fig. 9. Kinetics of generation of CO_2 reduction gas products: carbon monoxide *(a)*, methane *(b)* and hydrogen *(c)*.

Depending on the samples' nature different tendencies on a specific gas concentration are present. In particular, molecular hydrogen arises only after two hours in the presence of Au@SiC SA or SiC NW, but SiC SA does not initiate the production of H_2 over all the time of the kinetics. However, the chemical equilibrium at 1h and 2h impacted by SiC SA underwent intensive shift to monotonous CO concentration increase. But no CH_4 is formed after 1h by addition of SiC SA. Both SiC SA and Au@SiC SA demonstrated a significant decrease of CH_4 after 3h, which leads us to a conclusion that CO and CH_4 are found in a reciprocally proportional ratio dictated by SiC matrix. The gold nanoparticles influence the absolute values of the gas concentrations at the stable CO/CH_4 interrelation.

SiC NW feature in a stationary character to catalyze reduction of CO_2 to CO and CH_4 at equal CH_4/CO ratios with only double growth of H_2 after 3 h of the reaction. The sample is less active in contrast to Au@SiC SA and SiC SA to produce CO or CH_4.

The TEM images of Au@SiC SA have indicated a non-stable anchoring of Au nanodots onto SiC SA surface after 3 h of the reaction. The liquid media while stirring washed away gold nanodots due to porosity-deficient surface of SiC SA (Fig. 10). This suggests us to modify SiC NW with further involvement into the catalytic studies with a thoroughly developed strategy.

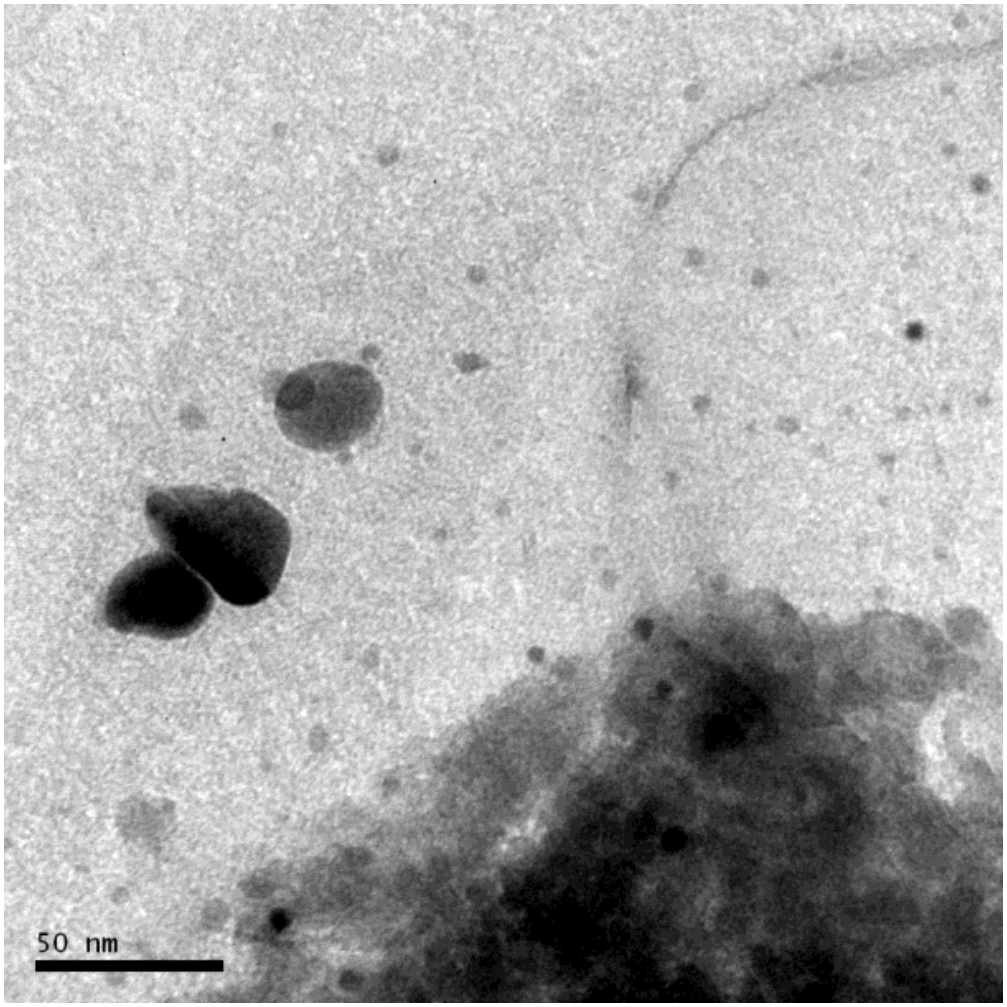

Fig. 10. The TEM image of Au@SiC SA after 3h of photcatalytic reaction.

5. Conclusões e perspectivas futuras

A novel material, such as silicon carbide nanowires, was studied as a photocatalyst. Additionally, gold-modified silicon carbide powder was obtained via advanced laser technique and analyzed by physicochemical methods. The formation of gold nanodots on a surface of powder silicon carbide was established. It has been shown that silicon carbide nanowires have a cubic crystalline structure and high specific surface area – 35 m^2/g. The porosity is fixed by meso- (59%) and macropores (38%). This advantage is reflected in a hydrogen generation and more pronounced CO_2 – CH_4 conversion in contrast to non-modified commercial silicon carbide at equal weights of both photocatalysts. The deposited gold nanodots on the commercial silicon carbide enable generation of molecular hydrogen and significant methane formation. Thus, silicon carbide nanowires are promising for further chemical modifications prescribed in WP3 and WP4.

The up-to-date results lead us to:

1) To study liquid solutions after photocatalytic reactions above for each of three samples in order to determine qualitative and quantitative content of organic compounds inside of solutions;

2) Modification of commercial silicon carbide powder and noew-synthsized nanowires by ruthenium, copper or cobalt nanodots via laser deposition;

3) Studying obtained materials for the carbon dioxide reduction under Xe-lamp or visible light orradiation;

4) To develop a technique of a high-thermal solid-phase process to synthesize porous silicon carbide to be exposed for biomedical application.

6. Referências

1. Dąbrowska, A., Huczko, A. & Katunin, A. SiC Nanofibres Produced by the Combustion Synthesis as the Nanocomposites Fillers. *Macromol. Symp.* **327,** 94–98 (2013).
2. Valentín, L. A. *et al.* A comprehensive study of thermoelectric and transport properties of β-silicon carbide nanowires. *J. Appl. Phys.* **114,** 184301 (2013).
3. Vijayan P, P. *et al.* Mechanical and thermal properties of epoxy/silicon carbide nanofiber

composites. *Polym. Adv. Technol.* **26,** 142–146 (2015).
4. Wang, C. *et al.* Recent progress in photocatalytic reduction of carbon dioxide utilizing titania catalysts. *Cailiao Daobao* **25,** 38–46 (2011).
5. Li, K., An, X., Park, K. H., Khraisheh, M. & Tang, J. A critical review of CO_2 photoconversion: Catalysts and reactors. *Catal. Today* **224,** 3–12 (2014).
6. Wang Johnathon and Yang, Y. Jeffrey and Biswas, Pratim, W.-N. and S. Comparison of CO_2 Photoreduction Systems: A Review. *Aerosol Air Qual. Res.* **14,** 533–549 (2014).
7. Voronin, E. F. *et al.* Interaction of poly(ethylene oxide) with fumed silica. *J. Colloid Interface Sci.* **279,** 326–340 (2004).
8. Nazarkovsky, M. A. *et al.* Titania-coated nanosilica-cobalt ferrite composites: Structure and photocatalytic activity. *J. Photochem. Photobiol. A Chem.* **319–320,** 40–52 (2016).
9. Nazarkovsky, M. A. *et al.* Synthesis and properties of zinc oxide photocatalyst by high-temperature processing of resorcinol- formaldehyde/zinc acetate mixture. *J. Photochem. Photobiol. A Chem.* **334,** 36–46 (2017).
10. Nguyen, C. & Do, D. D. A new method for the characterization of porous materials. *Langmuir* **15,** 3608–3615 (1999).
11. Nguyen, C. & Do, D. D. Effects of Probing Vapors and Temperature on the Characterization of Micro-Mesopore Size Distribution of Carbonaceous Materials. *Langmuir* **16,** 7218–7222 (2000).